as a whole show a pronounced dependence on the molar mass, as relaxation then has to propagate over larger and larger distances. Flow behavior is governed by these sluggish modes and therefore sets up the **terminal region**, i.e., the long time end, of the spectrum of relaxations.

The rates of the relaxatory modes in a sample do not cover the whole spectral range homogeneously, but usually one observes a separation into several zones where relaxation rates are accumulated. Each zone belongs to a group of processes with similar roots. It has become a convention to designate these different groups by Greek letters, α, β and γ, and to use the symbol α for the process with the lowest transition rates showing up at the highest temperature. On the other hand, the symbol γ is used for the processes observed at the low temperature end and this means those with the highest transition rates.

In the remaining part of this chapter, we discuss the properties of some major groups of relaxation processes in polymers as there are

- local processes, to be observed in the glassy state;
- cooperative processes in longer chain sequences that provide the basis for the elasticity of rubbers and the viscoelasticity of polymer melts;
- chain diffusion, which controls the flow behavior; and
- specific processes in partially crystalline states, associated with coupled motions of sequences in the crystallites and the amorphous regions.

6.3.1 Local Processes

Figure 6.7 shows the results of a dynamic shear experiment carried out on poly(cyclohexyl methacrylate) (PCHMA) in the glassy state. One observes a relaxation process that produces a loss maximum just in the frequency range of the mechanical spectrometer. With increasing temperature the position of the loss maximum shifts to higher values.

Considering the chemical constitution of PCHMA, there is an obvious assignment for this 'γ-process': It reflects the flip-motion between the chair-conformation and the boat-conformation of the cyclohexane sidegroup. Since this process changes the shape of the sidegroup, it couples to the applied shear field. The assignment is corroborated by the observation that this process shows up whenever a cyclohexyl group is attached to a polymer chain. The relaxation rates were similar for all samples investigated, as expected for a mode with local character.

Figure 6.8 shows the temperature dependence of the relaxation rate in an Arrhenius-plot. The data were obtained in several experiments on polyacrylates and poly(methylacrylates) with pendant cyclohexyl groups. The linearity of the plot is indicative of an activated process, the relaxation time being given by the Arrhenius law

$$\tau = \tau_0 \exp \frac{\tilde{A}}{\tilde{R}T} \,. \tag{6.93}$$

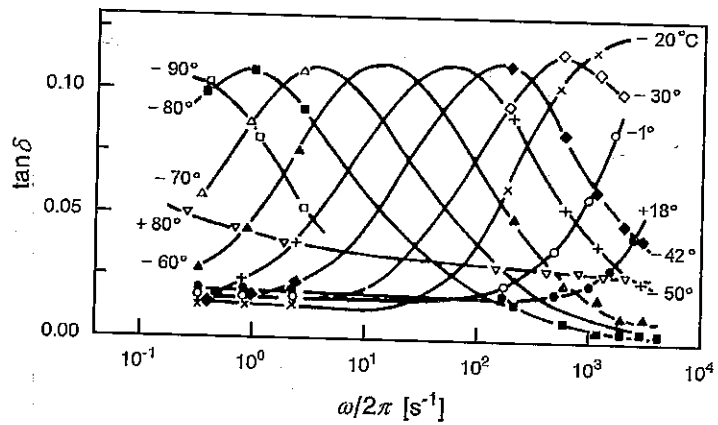

Fig. 6.7. Frequency dependence of the mechanical loss tangent measured for PCHMA at the indicated temperatures (after Heijboer [68])

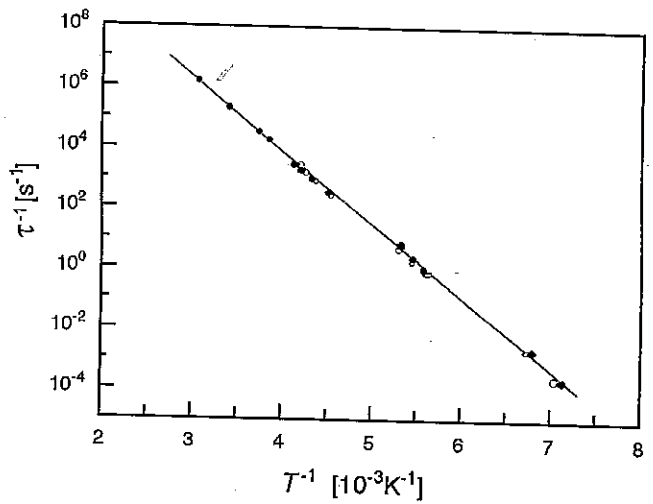

Fig. 6.8. Temperature dependence of the relaxation rates of the γ-process in polyacrylates (*open symbols*) and poly(methacrylates) (*filled symbols*) with pendant cyclohexyl groups. Data from Heijboer [69]

The relaxation rate τ^{-1} equals the rate of transitions between the two conformational states. The observed activation energy, $\tilde{A} = 47\,\mathrm{kJ\,mol^{-1}}$, therefore has to be identified with the height of the energy barrier that has to be passed over during a change.

A remarkable fact to be noted in Fig. 6.7 is the constancy in the peak amplitude and the shape of the loss curves when varying the temperature. This behavior, in combination with the regular temperature shift according to Arrhenius' law, opens the way for an alternative experimental procedure. Rather than carrying out frequency-dependent measurements at one temperature, loss curves may also be registered by temperature-dependent measurements at constant frequency. Figure 6.9 presents such measurements, and as can be seen, they provide equivalent information. The relationship between the relaxation rate and the temperature follows equally from both measurements by a registration of the loss maxima.

In the combination of frequency-dependent and temperature-dependent measurements, one can even go one step further, thereby establishing an important general procedure. For groups of relaxation processes that encompass a broader time range, it often happens that the experimentally limited frequency range of the experimental device is not large enough to include the curves completely. Measurements carried out at a sequence of different temperatures can provide the missing information. As indicated by our example, different parts of the loss curve are placed into the accessible frequency window on changing the temperature. This property can now be used to set up the complete loss curve by a synthesis. The sections obtained at the different temperatures can be coupled together by carrying out appropriate shifts along the log ω-axis, thus ending up in one continuous curve.

What is applied here is known in the literature as the **time–temperature superposition principle**. The result of the synthesis is called a **master curve**. For a thermally activated Debye process, the basis of the principle is

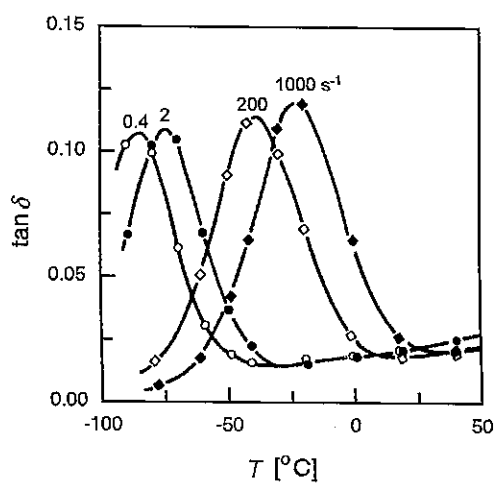

Fig. 6.9. Temperature dependent measurements of the loss tangent of the γ-process of PCHMA for several fixed frequencies $\omega/2\pi$ (after Heijboer [68])

easily seen. According to Eq. (6.65), the dynamic compliance and the dynam modulus are here functions of the product $\omega\tau$, or equivalently, of $\log(\omega\tau)$. we also use Eq. (6.93), we may then represent the compliance as a function a sum of terms

$$J(\log\omega\tau) = J\left(\log\omega + \log\tau_0 + \frac{\tilde{A}}{\tilde{R}T}\log e\right). \qquad (6.9$$

The expression tells us that there are two ways of achieving a change in namely either by a shift in $\log\omega$, or by a shift in T^{-1}. The effects of frequen and temperature thus appear as superposed, and Eq. (6.94) informs us abo the correspondences.

As a prerequisite for the construction of a master curve, the shape of t loss curve must remain constant under temperature variations. For the syst under discussion, this is obviously fulfilled. Measured curves coincide af appropriate shifts along the $\log\omega$-axis, as is shown in Fig. 6.10 for the r and imaginary part of the dynamic shear modulus. The example represe an ideal case, and here there is also no need for a synthesis of the cur from parts. In many other cases, however, construction of the master cu is the only means of exploring a group of relaxation processes in total. Ev

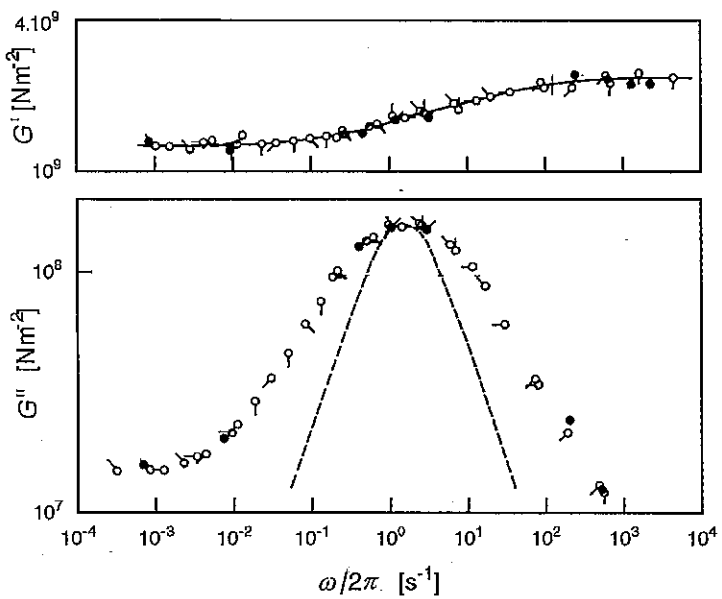

Fig. 6.10. Real and imaginary part of the dynamic shear modulus in the ra of the γ-process of PCHMA, synthesized as a master curve using measurements various temperatures. Curves represent the viscoelastic behavior at $-80\,°C$. *dashed curve* indicates a perfect Debye process. Data from Heijboer [69]

if one is not sure whether curve shapes are really temperature-independent, construction of a master curve remains useful as it can always provide a rough overall view, which is good for qualitative purposes.

Figure 6.10 shows also a comparison with the Debye process. We notice that the γ-process of the cyclohexyl groups does not agree with a single-time relaxation process, but exhibits some broadening. This may be caused by a coupling between adjacent sidegroups, as a conformational change in one sidegroup may well affect the neighbors. More specifically, the jump rate may depend on the conformations of the neighbors, which then would lead to a distribution of relaxation times, as is indicated by the broadened loss spectrum.

6.3.2 Glass–Rubber Transition and Melt Flow

Figure 6.11 presents creep curves, registered for a sample of polystyrene under shear stress at various temperatures between $-268\,^{\circ}\mathrm{C}$ and $296.5\,^{\circ}\mathrm{C}$. We observe a creep compliance that encompasses the enormously broad range of nine orders of magnitude. At the lowest temperatures, the mechanical properties are those of a glass. At the other limit, the high temperature end, the behavior is dominated by viscous flow as indicated by the characteristic linear increase of J with time. The transition from the solid-like to the liquid-like behavior occurs continuously, and importantly, obviously in a systematic manner. Indeed, the way curves change with temperature indicates that again time-temperature superposition is obeyed. Temperature variations result in shifts of the creep compliance along the $\log t$-axis, apparently without essential modifications in shape. The consequence is the same as for the just discussed local processes: On varying the temperature, different parts of $J(t)$ show up in the time-window of the experiment, and they can be reassembled to form a master curve. Applying this procedure yields the overall creep curve and it evidently has a shape as indicated schematically in Fig. 6.12. We can estimate the encompassed total time range by roughly summing up the time ranges of the sections included and find an enormous extension of about 20 orders of magnitude.

$J(t)$ has a characteristic shape composed of several parts. Subsequent to the glassy range with a solid-like compliance in the order of $10^{-9}\,\mathrm{N^{-1}\,m^2}$, an additional anelastic deformation emerges and eventually leads to a shear compliance in the order of $10^{-5}\,\mathrm{N^{-1}\,m^2}$. The latter value is typical for a rubber. For a certain time a plateau is maintained but then there finally follows a steady linear increase of J, as is indicative for viscous flow. The displayed creep curve of polystyrene is not a peculiar one and may be regarded as representative for all amorphous, i.e., noncrystalline polymers. One always finds these four parts in

- a glassy region;
- the glass–rubber transition, often also called the 'α-process',

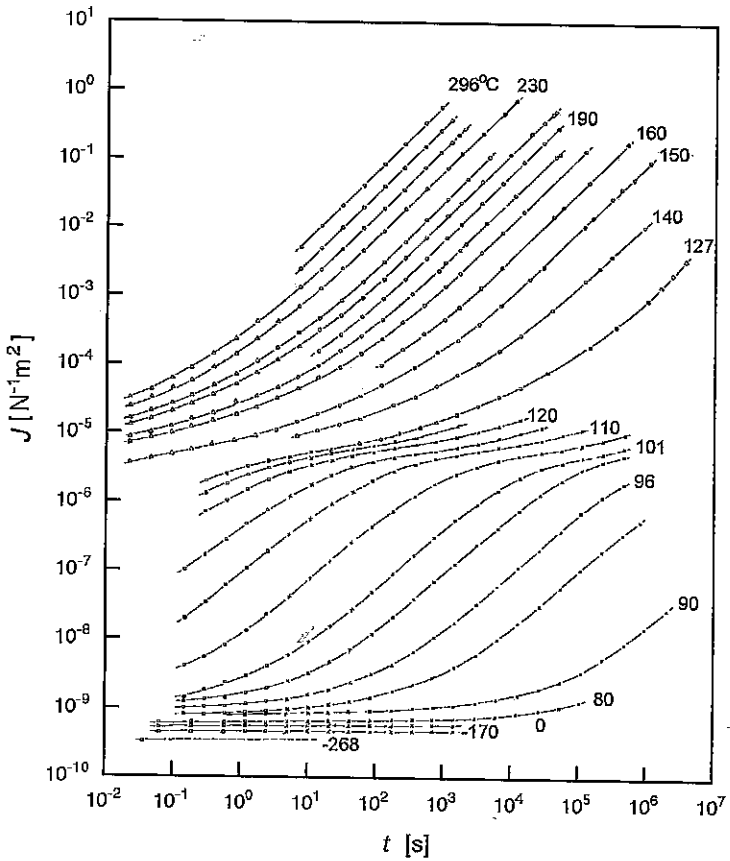

Fig. 6.11. Creep compliance of PS ($\overline{M}_\mathrm{w} = 3.85 \times 10^5\,\mathrm{g\,mol^{-1}}$), as measured at the indicated temperatures. Data from Schwarzl [70]

- a rubber–elastic plateau; and
- the terminal flow range.

These are the basic ingredients determining the mechanical properties of amorphous polymers and we now discuss them in a brief overview.

A first important conclusion can be drawn immediately; it concerns the nature of the main part, the glass–rubber transition. As we find a systematic shift of the time range of the transition with temperature, it is obvious that we are dealing here with a purely kinetical phenomenon rather than with a structural transition like the melting process or a solid-solid phase change. Curves demonstrate that whether a sample reacts like a glass or a rubber is just a question of time. Temperature enters only indirectly, in that it determines the characteristic time that separates glassy from rubbery behavior.

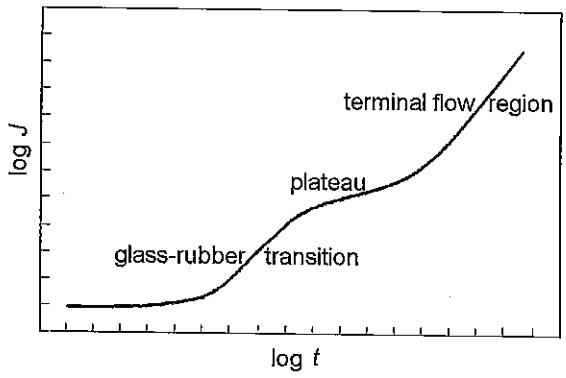

Fig. 6.12. General shape of the complete creep curve of PS, as suggested by the appearance of the different parts shown in Fig. 6.11

In Chap. 9, we will discuss the properties of rubbers. These are networks, composed of chemically cross-linked macromolecules. Owing to the weak restoring forces, application of stress here induces a deformation that is very large compared to solids. The observation of a plateau in the creep compliance at a height comparable to the compliance of rubbers indicates that a polymer melt actually resembles a temporary network. This behavior expresses a major property specific for polymeric liquids: These include chain entanglements, i.e., constraints for the motion arising from the chain connectivity, which act like cross-links. Different from true cross-links of chemical nature, entanglements are only effective for a limited time during which they are able to suppress flow. This time becomes apparent in the creep curve as the end of the plateau region.

Subsequent to the plateau, flow sets in. As is intuitively clear, the time needed for the chain disentangling increases with the molar mass and this shows up in a corresponding broadening of the plateau. Results of dynamic-mechanical experiments on polystyrene, presented later in Fig. 6.16, exemplify the behavior. The data also indicate a lower limit: When decreasing the molar mass one reaches a point, where the plateau vanishes. Then the glass–rubber transition and the terminal flow region merge together. Absence of the plateau means the absence of an entanglement network. The observation tells us that entanglement effects only exist above a certain minimum molar mass. For each polymer one finds for that a characteristic value, known as the **molar mass at the entanglement limit**.

The measurements at high temperatures in Fig. 6.11 indicate a viscous flow with a constant creep rate, determined by a viscosity η_0

$$\frac{\mathrm{d}J}{\mathrm{d}t} \propto \frac{1}{\eta_0} \,. \tag{6.95}$$

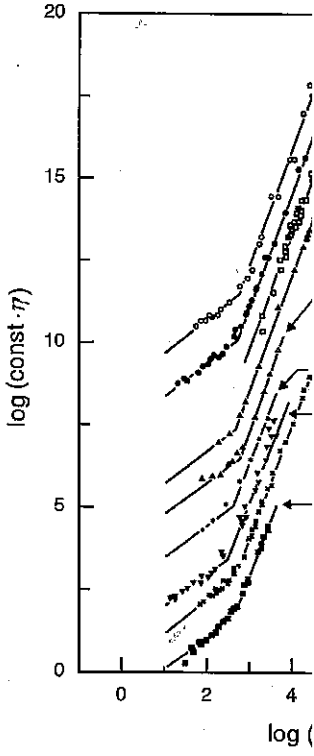

Fig. 6.13. Molecular weight dependence
cated polymers. For better comparison cu
vertical directions. Data from Berry and

As the flow velocity relates to the dise
melt viscosity. Indeed, η_0 and the disen
the same dependence on the molar m
viscosity measurements for various poly
behavior

$$\eta_0 \propto$$

is generally observed. One finds two reg
nent ν and a cross-over at a **critical mo**
M_c one has $\nu = 1$; above M_c one obser
ments are further extended, up to the
finally observes an exponent $\nu = 3$. Fi
for 1,4-polyisoprene (PI), for molar ma

Importantly, as is also shown by Fig
response separated by the rubber–elas
dependence. In contrast to the termina

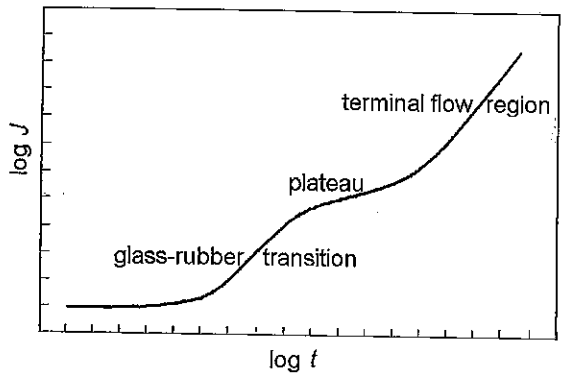

6.12. General shape of the complete creep curve of PS, as suggested by the arance of the different parts shown in Fig. 6.11

Chap. 9, we will discuss the properties of rubbers. These are net-s, composed of chemically cross-linked macromolecules. Owing to the restoring forces, application of stress here induces a deformation that y large compared to solids. The observation of a plateau in the creep liance at a height comparable to the compliance of rubbers indicates a polymer melt actually resembles a temporary network. This behavior sses a major property specific for polymeric liquids: These include chain glements, i.e., constraints for the motion arising from the chain connec-, which act like cross-links. Different from true cross-links of chemical e, entanglements are only effective for a limited time during which they ble to suppress flow. This time becomes apparent in the creep curve as id of the plateau region.

bsequent to the plateau, flow sets in. As is intuitively clear, the time d for the chain disentangling increases with the molar mass and this up in a corresponding broadening of the plateau. Results of dynamic-anical experiments on polystyrene, presented later in Fig. 6.16, exemplify ehavior. The data also indicate a lower limit: When decreasing the molar one reaches a point, where the plateau vanishes. Then the glass–rubber tion and the terminal flow region merge together. Absence of the plateau s the absence of an entanglement network. The observation tells us that glement effects only exist above a certain minimum molar mass. For each ier one finds for that a characteristic value, known as the **molar mass e entanglement limit.**

ie measurements at high temperatures in Fig. 6.11 indicate a viscous vith a constant creep rate, determined by a viscosity η_0

$$\frac{\mathrm{d}J}{\mathrm{d}t} \propto \frac{1}{\eta_0} \,. \tag{6.95}$$

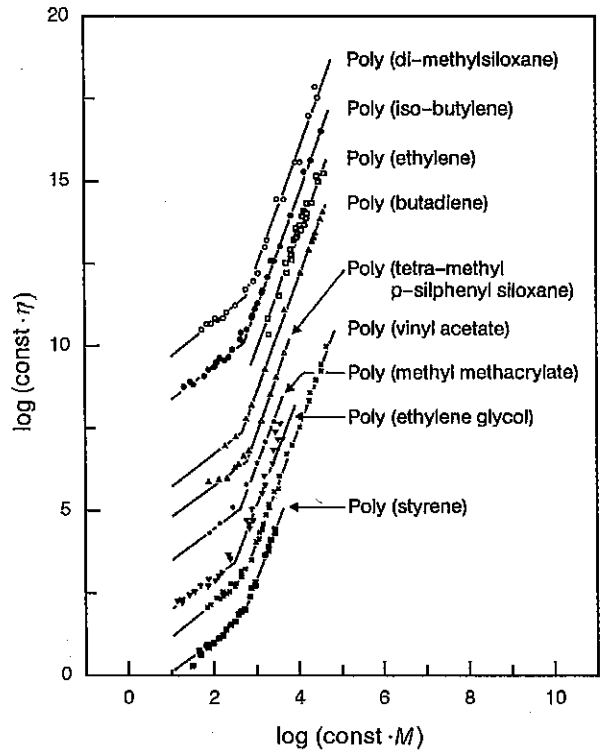

Fig. 6.13. Molecular weight dependence of the viscosity as observed for the indicated polymers. For better comparison curves are suitably shifted in horizontal and vertical directions. Data from Berry and Fox [71]

As the flow velocity relates to the disentangling time, this also holds for the melt viscosity. Indeed, η_0 and the disentangling time for entangled melts show the same dependence on the molar mass. Figure 6.13 collects the results of viscosity measurements for various polymers. As should be noted, a power law behavior

$$\eta_0 \propto M^{\nu} \tag{6.96}$$

is generally observed. One finds two regions, with different values of the exponent ν and a cross-over at a **critical molar mass** M_c. For molar masses below M_c one has $\nu = 1$; above M_c one observes $\nu \approx 3.2-3.6$. If viscosity measurements are further extended, up to the range of ultra-high molar masses, one finally observes an exponent $\nu = 3$. Figure 6.14 presents such measurements for 1,4-polyisoprene (PI), for molar masses up to $\overline{M}_w = 3 \times 10^6\,\mathrm{g\,mol^{-1}}$.

Importantly, as is also shown by Fig. 6.16, the two parts of the mechanical response separated by the rubber-elastic plateau differ in their molar mass dependence. In contrast to the terminal flow region, the glass–rubber transi-

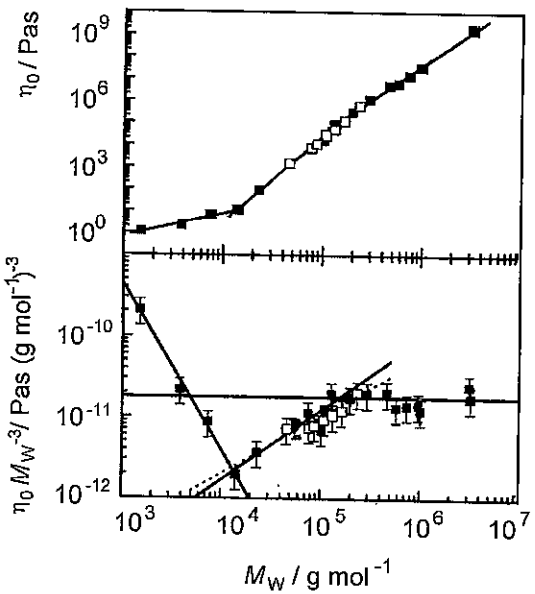

Fig. 6.14. Molar mass dependence of the zero shear rate viscosity of PI. The *lower figure* indicates for $\overline{M}_w > 2 \times 10^5$ g mol^{-1} a power law $\eta_0 \propto \overline{M}_w^3$. The critical molar mass as determined by the location of the break is $M_c = 1.3 \times 10^4$ g mol^{-1}. From Pyckhout-Hintzen et al. [72]

tion remains largely unaffected by the molar mass. The findings teach us that chain equilibration in reaction to an applied field takes place as a two-step process with a finite delay time in between. In the first step, equilibration by relaxatory modes only includes chain sequences up to a certain length, which is determined by the distance between the entanglements. As this distance is independent of M, this holds likewise for the characteristic time of this first step. Further relaxation is postponed until a chain extricates itself from the **tube** formed by the other surrounding molecules and this process is of course strongly affected by the molar mass.

As explained in the first part of this chapter, the viscoelastic properties of polymers may also be studied by stress relaxation experiments or dynamic mechanical measurements. Since all response functions are interrelated, the mentioned ingredients of the mechanical behavior of amorphous polymers show up in the other experiments as well. To give an example, Fig. 6.15 displays the time-dependent tensile modulus registered for polyisobutylene (PIB). Measurements were again conducted for a series of temperatures. As expected, data show the glass–rubber transition (for temperatures in the range 190–220 K), followed by a plateau (around 230 K) and finally the onset of flow. The right-hand side presents the composite master curve, set up by shifting

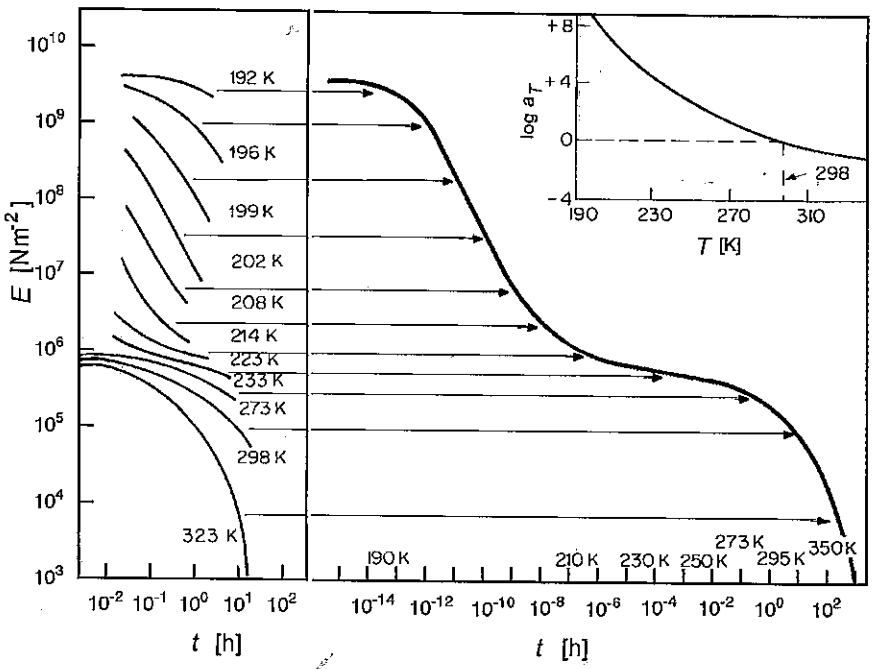

Fig. 6.15. Time-dependent tensile modulus of PIB. Measurements at the indicated temperatures (*left*) and master curve, constructed for a reference temperature $T = 298$ K (*right*). The *insert* displays the applied shifts. Data from Castiff and Tobolsky [73]

the partial curves as indicated by the arrows. The shifts along the $\log t$-axis, which have to be carried out when going from the master curve to the measured parts, are displayed in the insert. In the construction of the master curve the time-dependent modulus obtained at 298 K was kept fixed, while all other curves were displaced. The shift factor, denoted $\log a_T$, is zero at this reference temperature. The result represents the complete time-dependent shear modulus at the reference temperature. Comparable to the creep compliance in Fig. 6.12, this tensile modulus again encompasses a huge range of about 20 orders of magnitude in time.

Regarding the large number of conformational changes that must take place if a rubber is to be extended, the glass–rubber transition cannot equal a single-time relaxation process and this is shown by the curve shapes. To describe $E(t)$, empirical equations that often provide good data fits exist. A first one is concerned with the beginning of the transition range. It is known as the **Kohlrausch–Williams–Watts** (KWW) **function** and has the form of a **stretched exponential function**

$$E(t) \propto \exp - \left(\frac{t}{\tau}\right)^{\beta} . \qquad (6.97)$$

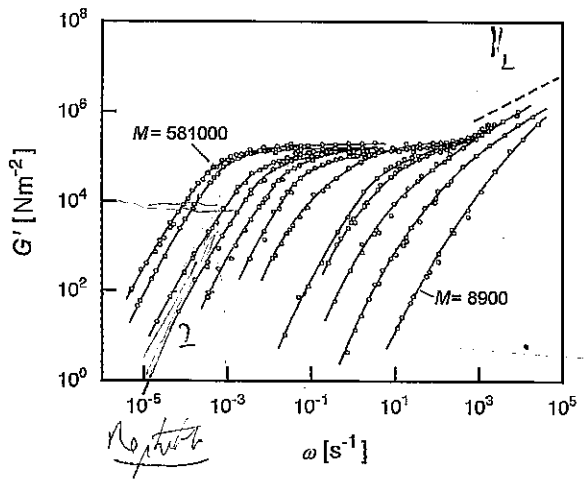

Fig. 6.16. Storage shear moduli measured for a series of fractions of PS with different molar masses in the range $M = 8.9 \times 10^3$ to 5.81×10^5 g mol^{-1}. The *dashed line in the upper right corner* indicates the slope corresponding to the power law Eq. (8.82) derived for the Rouse model of the glass transition. Data from Onogi et al. [74]

The KWW function employs two parameters: τ sets the time scale and β determines the extension in time of the decay process. For values $\beta < 1$ a broadening results, as is always observed for the glass–rubber transition. Typical values are in the order $\beta \simeq 0.5$. The KWW function holds only at the beginning, i.e., in the short-time range of the glass–rubber transition. Subsequently, there often follows a power law

$$E(t) \propto t^{-\nu} \,. \tag{6.98}$$

Experimentally it is indicated by a linear range in the center, when using a log–log plot. Typical values of the exponent are $\nu \simeq 0.5$.

Figure 6.16 presents, as a third example, results of dynamic-mechanical measurements. They were obtained for a series of monodisperse polystyrenes, i.e., fractions with sharp molar masses. The curves depict the frequency dependence of the storage shear modulus, $G'(\omega)$. As we note, the order of appearance of the viscous flow and the α-process is reversed when compared to the time-dependent measurements. The flow-dominated long-time behavior emerges first at low frequencies, whereas an investigation of the rubber–glass transition requires measurements at the high frequency end. The plateau appears in between. Its width varies systematically with the molar mass, as has already been mentioned and discussed. There is no plateau at all for the sample with the lowest molar mass ($M = 8.9 \times 10^3$ g mol^{-1}), but after its first appearance, it widens progressively with further increasing molar masses.

Low Frequency Properties of Polymer Melts

Also of interest in Fig. 6.16 is the finding that the shapes of curves in th terminal region remain similar to each other for all molar masses. More specif ically, within the limit of low frequencies, a constant slope emerges, indicatin a power law $G'(\omega) \propto \omega^2$. It is possible to explain this asymptotic behavio and to relate it to the properties of flowing polymer melts.

For a Newtonian low molar mass liquid, knowledge of the viscosity is full sufficient for the calculation of flow patterns. Is this also true for polymeri liquids? The answer is no under all possible circumstances. Simple situation are encountered, for example, in dynamical tests within the limit of low fre quencies or for slow steady state shears and even in these cases, one has t include one more material parameter in the description. This is the **recover able shear compliance**, usually denoted by J_e^0 and it specifies the amoun of recoil observed in a creep recovery experiment when the load is removed J_e^0 relates to the elastic and anelastic parts in the deformation and has to b accounted for in all calculations. Experiments show that, at first, for $M < M_c$ J_e^0 increases linearly with the molar mass and then reaches a constant valu that essentially agrees with the plateau value of the shear compliance.

At higher strain rates more complications arise. There the viscosity is n longer constant and shows a decrease with increasing rate, which is com monly addressed as **shear-thinning**. We will discuss this effect and relate phenomena in Chap. 9 when dealing with non-linear behavior. In this section the focus is on the limiting properties at low shear rates, as expressed by th **zero shear rate viscosity**, η_0, and the recoverable shear compliance at zer shear rate, J_e^0.

Our concern is to find out how the characteristic material parameters η and J_e^0 are included in the various response functions. To begin with, conside a perfectly viscous system in a dynamic-mechanical experiment. Here th dynamic shear compliance is given by

$$J = \mathrm{i}\frac{1}{\eta_0 \omega} \,. \tag{6.99}$$

This is seen when introducing the time dependencies

$$\sigma_{zx} = \sigma_{zx}^0 \exp(-\mathrm{i}\omega t) \,,$$
$$e_{zx} = J\sigma_{zx}^0 \exp(-\mathrm{i}\omega t)$$

into the basic equation for Newtonian liquids

$$\sigma_{zx} = \eta_0 \frac{\mathrm{d}e_{zx}}{\mathrm{d}t} \,, \tag{6.100}$$

which results in

$$\sigma_{zx}^0 \exp(-\mathrm{i}\omega t) = -\eta_0 \mathrm{i}\omega J \sigma_{zx}^0 \exp(-\mathrm{i}\omega t) \,. \tag{6.101}$$

In a polymer melt, the viscous properties of Newtonian liquids combine with elastic forces. The latter contribute a real part to the dynamic shear compliance, to be identified with J_e^0:

$$J'(\omega \to 0) = J_e^0 \,. \tag{6.102}$$

Combining Eqs. (6.99) and (6.102) gives the dynamic shear compliance of polymeric fluids in the limit of low frequencies

$$J(\omega \to 0) = J_e^0 + \mathrm{i}\frac{1}{\eta_0 \omega} \,. \tag{6.103}$$

As we can see, η_0 and J_e^0 show up directly and separately, in the limiting behavior of J' and J''.

The dynamic shear modulus follows as

$$\begin{aligned} G(\omega \to 0) &= \frac{1}{J(\omega \to 0)} = \frac{\eta_0 \omega}{\eta_0 \omega J_e^0 + \mathrm{i}} \\ &= \frac{\eta_0^2 \omega^2 J_e^0 - \mathrm{i}\eta_0 \omega}{(\eta_0 \omega J_e^0)^2 + 1} \,, \end{aligned} \tag{6.104}$$

giving

$$G'(\omega \to 0) = J_e^0 \eta_0^2 \omega^2 \tag{6.105}$$

in agreement with Fig. 6.16, and

$$G''(\omega \to 0) = \eta_0 \omega \,. \tag{6.106}$$

We thus find characteristic power laws also for the storage and the loss modulus that again include J_e^0 and η_0 in a well-defined way.

One may wonder if η_0 and J_e^0 can also be deduced from the time-dependent response functions, as for example, from $G(t)$. Indeed, direct relationships exist, expressed by the two equations

$$\eta_0 = \int_0^\infty G(t)\,\mathrm{d}t \tag{6.107}$$

and

$$J_e^0 \eta_0^2 = \int_0^\infty G(t) t\,\mathrm{d}t \,. \tag{6.108}$$

The first relation follows immediately from Boltzmann's superposition principle in the form of Eq. (6.38) when applied to the case of a deformation with constant shear rate $\dot{e}_{zx}$. We have

$$(\mathrm{d}x \widehat{=}) \, \mathrm{d}e_{zx} = \dot{e}_{zx}\,\mathrm{d}t \tag{6.109}$$

and thus

$$(\psi \widehat{=}) \; \sigma_{zx} = \dot{e}_{zx} \int_{t'=-\infty}^{t} G(t-t')\,\mathrm{d}t' = \dot{e}_{zx} \int_{t''=0}^{\infty} G(t'')\,\mathrm{d}t'' \,. \tag{6.11}$$

Since per definition

$$\sigma_{zx} = \eta_0 \dot{e}_{zx} \,,$$

we find

$$\eta_0 = \int_{t=0}^{\infty} G(t)\,\mathrm{d}t \,.$$

To derive the second equation, we consider a dynamic-mechanical experime and treat it again on the basis of Boltzmann's superposition principle, writi

$$\sigma_{zx} = \int_{t'=-\infty}^{t} G(t-t')\dot{e}_{zx}(t')\,\mathrm{d}t' \,. \tag{6.11}$$

Introducing

$$e_{zx}(t) = e_{zx}^0 \exp(-\mathrm{i}\omega t) \tag{6.11}$$

and

$$\sigma_{zx}(t) = G(\omega) e_{zx}(t) \tag{6.11}$$

we obtain

$$G(\omega) = -\int_{t''=0}^{\infty} G(t'')\mathrm{i}\omega \exp(\mathrm{i}\omega t'')\,\mathrm{d}t'' \,, \tag{6.11}$$

setting $t'' = t - t'$. In the limit $\omega \to 0$ we use the series expansion

$$G(\omega \to 0) = \int_{t''=0}^{\infty} G(t'')(-\mathrm{i}\omega + \omega^2 t'' + \ldots)\,\mathrm{d}t'' \,, \tag{6.11}$$

giving

$$G'(\omega \to 0) = \omega^2 \int_{t=0}^{\infty} G(t) t\,\mathrm{d}t \,. \tag{6.11}$$

A comparison with Eq. (6.105) yields Eq. (6.108).

Combination of Eqs. (6.107) and (6.108) can be used for estimating t average time of stress decay subsequent to a sudden shear deformation a melt. We introduce this time, denoted by $\bar{\tau}$, as

$$\bar{\tau} = \frac{\int_{t=0}^{\infty} G(t)t\,\mathrm{d}t}{\int_{t=0}^{\infty} G(t)\,\mathrm{d}t}\,, \tag{6.117}$$

and then obtain simply

$$\bar{\tau} = J_\mathrm{e}^0\eta_0\,. \tag{6.118}$$

Equation (6.118) for the mean viscoelastic relaxation time may be applied for both non-entangled and entangled melts and yields different results for the two cases. For non-entangled melts, i.e., $M < M_\mathrm{c}$, we have $J_\mathrm{e}^0 \propto M$ and $\eta_0 \propto M$, hence

$$\bar{\tau} \propto M^2\,. \tag{6.119}$$

For molar masses above the entanglement limit, i.e., $M > M_\mathrm{c}$, one finds $J_\mathrm{e}^0 = \text{const}$ and $\eta_0 \propto M^\nu$ with $\nu = 3\text{–}3.6$, therefore,

$$\bar{\tau} \propto \eta_0 \propto M^\nu \text{ with } \nu = 3\text{–}3.6\,. \tag{6.120}$$

Vogel–Fulcher Law and the WLF Equation

We turn now to another point and consider the temperature dependence. Recall that the data indicate the validity of time-temperature or frequency-temperature superposition. This has an important implication: The findings show that the processes comprising the terminal flow region and the glass–rubber transition change with temperature in the same manner. Particularly suited for the description of this common temperature dependence is the shift parameter $\log a_T$. We introduced it in connection with the construction of the master curves, but it also has a well-defined physical meaning. This becomes revealed when we look at the equations valid in the terminal range, Eqs. (6.105) and (6.106). It is to be noted that ω and η_0 enter into the expressions for the dynamic modulus and the dynamic compliance not separately, but only as a product. As temperature only affects η_0, we conclude that a_T and η_0 must be proportional quantities. The exact relationship follows when taking into account that shift parameters always relate to a certain reference temperature. Let this reference temperature be T_0. Then a_T is given by

$$a_T = \frac{\eta_0(T)}{\eta_0(T_0)}\,. \tag{6.121}$$

With the aid of a_T we can express response functions at any temperature in terms of the respective response function at T_0. Explicitly, for the dynamical shear modulus, the following relation holds:

$$G(T,\omega) = G(T_0, a_T\omega)\,, \tag{6.122}$$

or for a logarithmic frequency scale

$$G(T,\log\omega) = G(T_0,\log\omega + \log a_T)\,. \tag{6.123}$$

In correspondence to this, we write for the time-dependent shear modulus

$$G(T,t) = G\left(T_0, \frac{t}{a_T}\right)\,, \tag{6.124}$$

or

$$G(T,\log t) = G(T_0,\log t - \log a_T)\,. \tag{6.125}$$

The uniform temperature dependence implies a joint rescaling of the relaxation times of all modes in both the glass transition range and the terminal flow region, and one may wonder how this might arise. One should be aware that these modes vary greatly in their spatial extensions, which begin with the length of a Kuhn segment and go up to the size of the whole chain, and also vary in character, as they include intramolecular motions as well as diffusive movements of the whole chain, and nevertheless, all modes behave uniformly. There seems to be only one possible conclusion: The temperature dependence must be a property of the individual segments. Since all modes are based on the motion of segments, their mobility affects each mode alike. There is a notion that suitably expresses this property and this is the **segmental frictional coefficient**. We will introduce it in the next chapter, in the treatment of microscopic dynamics. For the moment, it is sufficient to say that frictional forces that act in identical manner on all the segments exist. They uniformly control the kinetics of all the relaxatory modes of the chains. The common temperature dependence of all relaxatory modes in the α-transition range and the terminal zone, and thus of the viscosity, just reflects that of the segmental frictional force.

Equation (6.121) relates a_T to the temperature dependence of the viscosity. Numerous experiments were carried out to measure this function. They led to a specific result. As it turns out, for the majority of polymer systems, $\eta_0(T)$ is well-represented by an empirical equation known as the **Vogel–Fulcher law**. It has the form

$$\eta_0(T) = B\exp\frac{T_\mathrm{A}}{T - T_\mathrm{V}}\,. \tag{6.126}$$

In addition to the prefactor B two parameters are included, namely the **activation temperature** T_A and the **Vogel temperature** T_V. The introduction of the latter makes up the difference to Arrhenius' law.

The function $\eta_0(T)$, as formulated by the Vogel–Fulcher law, includes a singularity at $T = T_\mathrm{V}$. However, whether the viscosity really diverges as T approaches T_V cannot be checked by any experiment. Measurements of viscosities always come to an end about 50 K above T_V, because η_0 is then already very large, reaching values in the order of 10^{13} poise. Notwithstanding the fact that the point of divergence is out of reach, validity of the Vogel–Fulcher equation is well-established since effects of a finite Vogel temperatur

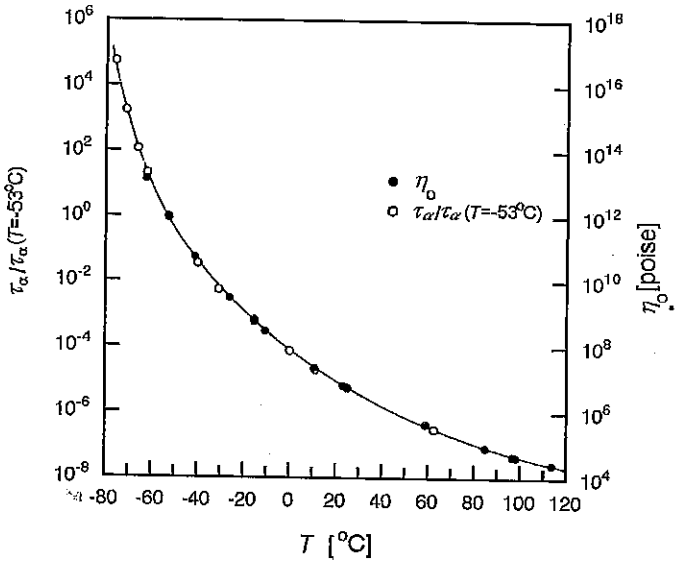

Fig. 6.17. Temperature dependencies of the viscosity η_0 of PIB (*open symbols, right axis*) and of the relaxation time of the α-process τ_α (*filled symbols, left axis*). Both correspond to a Vogel–Fulcher function (*continuous line*). Data from Plazek et al. [75]

are clearly observable also in the range of accessible temperatures. There, the function $\eta_0(T)$ exhibits a characteristic curvature that distinguishes it from Arrhenius behavior. Figure 6.17 depicts, as an example, results obtained for polyisobutylene (PIB). An increase to high values of η_0 is observed at low temperatures and it can be described by a Vogel–Fulcher function, as given by the continuous line. The figure also includes the temperature dependence of the characteristic time τ_α of the glass–rubber transition. It is given by

$$\tau_\alpha = \tau_0 \exp \frac{T_\mathrm{A}}{T - T_\mathrm{V}} \tag{6.127}$$

with the same values for T_A and T_V as in Eq. (6.126).

Having an equation for the temperature dependence of the viscosity, we may also formulate the shift factor $\log a_T$. Equations (6.126) and (6.121) yield

$$\begin{aligned} \log a_T &= \log \mathrm{e} T_\mathrm{A} \left(\frac{1}{T - T_\mathrm{V}} - \frac{1}{T_0 - T_\mathrm{V}} \right) \\ &= \log \mathrm{e}(-T_\mathrm{A}) \frac{T - T_0}{(T_0 - T_\mathrm{V})(T - T_\mathrm{V})} \\ &= \log \mathrm{e} \frac{(-T_\mathrm{A})}{T_0 - T_\mathrm{V}} \frac{T - T_0}{T - T_0 + (T_0 - T_\mathrm{V})} \,. \end{aligned} \tag{6.128}$$

This is usually expressed as

$$\log a_T = -C_1 \frac{T - T_0}{T - T_0 + C_2} \,, \tag{6.129}$$

introducing two parameters, C_1 and C_2, defined as

$$C_1 = \log \mathrm{e} \frac{T_\mathrm{A}}{T_0 - T_\mathrm{V}} \quad \text{and} \quad C_2 = T_0 - T_\mathrm{V} \,. \tag{6.130}$$

Equation (6.129) was postulated by Williams, Landel and Ferry and is well-known in the literature under the abbreviated name **WLF equation.**

When master curves are constructed one chooses in most cases the glass transition temperature T_g as reference temperature. T_g is obtained by a standard calorimetric or volumetric measurement, as explained in Sect. 6.3.3. It is found that, for this choice of T_0, the parameters C_1 and C_2 of the WFL equation have values which are bound to certain ranges, namely

$$\begin{aligned} C_1 &= 14 - 18, \\ C_2 &= (30 - 70)\ \mathrm{K} \,. \end{aligned}$$

The values of C_2 indicate that T_V is located (30−70) K below T_g.

The Dielectric α-Process and the Normal Mode

The two groups of relaxatory modes that in mechanical relaxation experiments lead to the α-transition and the final viscous flow also emerge in the dielectric response.

Figure 6.18 presents, as a first example, the frequency dependencies of the real and imaginary part of the dielectric constant, obtained for poly(vinylacetate) (PVA) at the indicated temperatures. One observes a strong relaxation process.

Figure 6.19 displays the temperature dependence of the relaxation rate, as derived from the maxima of the loss curves. For a comparison it also includes the temperature dependencies of the loss maxima of the mechanical α-process, as observed in measurements of either $J''(\omega)$ or $G''(\omega)$. As we can see, the dielectric relaxation rates are located intermediately between the rates obtained in the mechanical experiments and, importantly, all three temperature dependencies are similar, the rates differing only by constant factors. The assignment of this dielectric relaxation process is therefore obvious: It originates from the same group of processes as the mechanical α-process and thus is to be addressed as the dielectric α-process.

There are other polymers that in addition show the chain disentangling associated with the flow transition. An example is given by *cis*-polyisoprene (PIP). Figure 6.20 depicts the dielectric loss ε'' in a three-dimensional representation of the functional dependence on frequency and temperature. Two

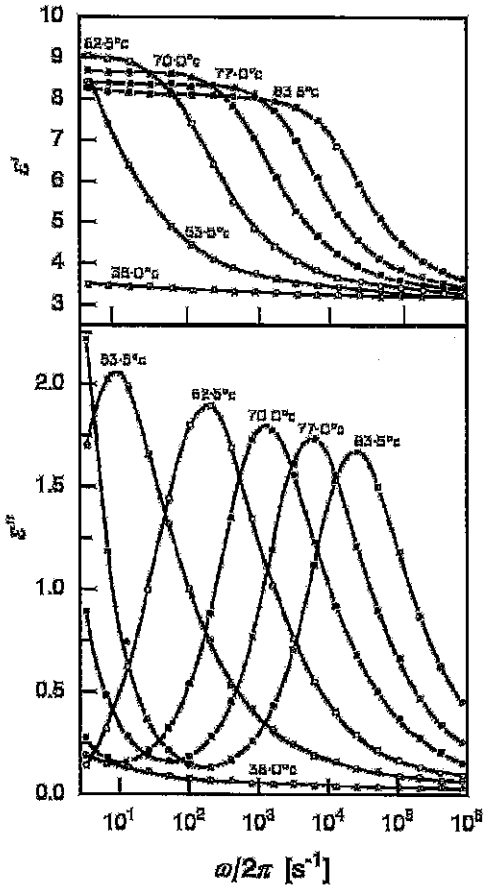

Fig. 6.18. Dielectric α-process in PVA. Data from Ishida et al. [76]

relaxation processes show up. The one with the higher frequency again represents the α-process, the other is called the **normal mode**, for reasons to be seen below.

To learn more about the two processes, it is instructive to check for the molar mass dependencies. In fact, one here finds a characteristic difference. The results of studies on a set of samples with different molar mass are displayed in Fig. 6.21. We observe that the α-process is molar mass independent, whereas the normal mode shows pronounced changes. Figure 6.22 depicts these changes in a plot of the relaxation time τ of the normal mode in dependence on the molar mass. Data demonstrate the validity of a power law,

$$\tau \propto M^{\nu} \ ,$$

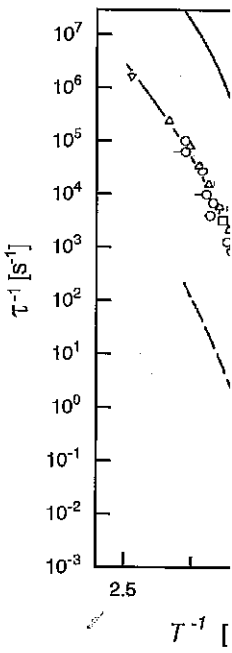

Fig. 6.19. Frequency–temperature locatio
symbols) of PVA, compared to the maxima
line) observed in mechanical experiments. C

with two different values for the exponer

$$\nu = 3.7 \quad \text{for} \quad M$$

and

$$\nu = 2 \quad \text{for} \quad M <$$

The cross-over from one to the other regi
curve.

We have already met such a molar m
(6.120), when formulating the average vi
mer melts. Roughly speaking, $\bar{\tau}$ gives the
plete conformational reorganization. Thi
the end-to-end distance vector of the cha
shows up in the dielectric normal mode.

The question arises as to why *cis*-pol
acetate), shows the chain reorientation ir
becomes clear when we look at the chemi

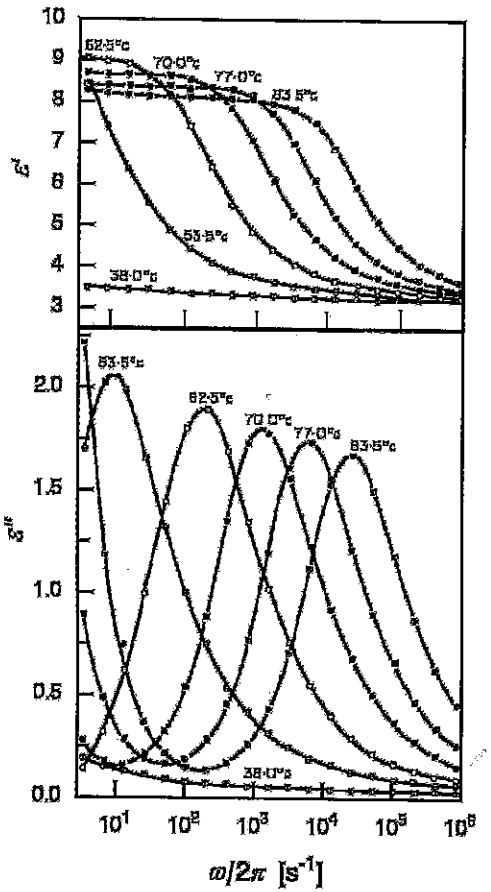

Fig. 6.18. Dielectric α-process in PVA. Data from Ishida et al. [76]

ıtion processes show up. The one with the higher frequency again repre- the α-process, the other is called the **normal mode**, for reasons to be ɔelow.

ɔ learn more about the two processes, it is instructive to check for the mo- ıss dependencies. In fact, one here finds a characteristic difference. The s of studies on a set of samples with different molar mass are displayed in .21. We observe that the α-process is molar mass independent, whereas ɔrmal mode shows pronounced changes. Figure 6.22 depicts these changes ɔlot of the relaxation time τ of the normal mode in dependence on the mass. Data demonstrate the validity of a power law,

$$\tau \propto M^{\nu} ,$$

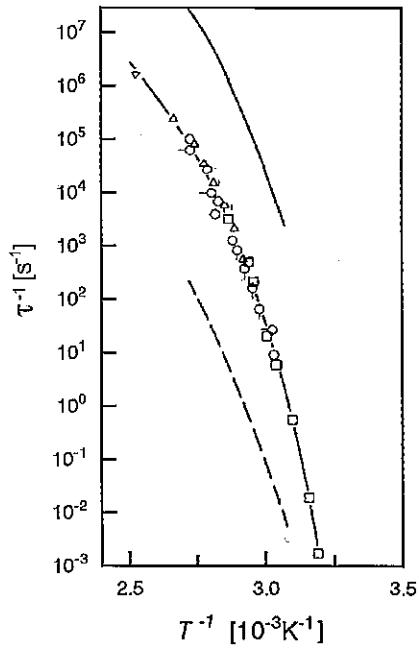

Fig. 6.19. Frequency–temperature locations of the dielectric loss maxima (*open symbols*) of PVA, compared to the maxima of G'' (*continuous line*) and J'' (*broken line*) observed in mechanical experiments. Collection of data published in [77]

with two different values for the exponent,

$$\nu = 3.7 \quad \text{for} \quad M > 10^4\,\mathrm{g\,mol^{-1}}$$

and

$$\nu = 2 \quad \text{for} \quad M < 10^4\,\mathrm{g\,mol^{-1}} .$$

The cross-over from one to the other regime shows up as a sharp bend in the curve.

We have already met such a molar mass dependence in Eqs. (6.119) and (6.120), when formulating the average viscoelastic relaxation time $\bar{\tau}$ of polymer melts. Roughly speaking, $\bar{\tau}$ gives the time required by a chain for a complete conformational reorganization. This also implies a full reorientation of the end-to-end distance vector of the chain. This is exactly this motion that shows up in the dielectric normal mode.

The question arises as to why *cis*-polyisoprene, different from poly(vinylacetate), shows the chain reorientation in its dielectric spectrum. The reason becomes clear when we look at the chemical constitution of polyisoprene, and

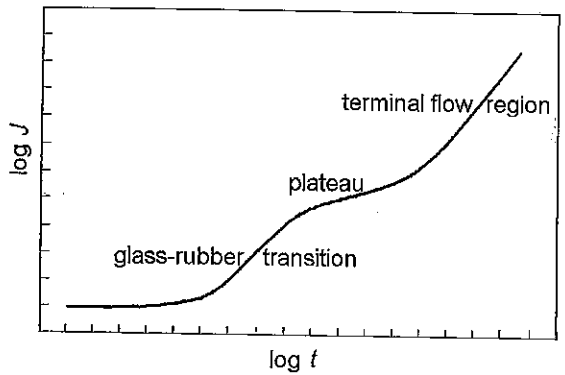

6.12. General shape of the complete creep curve of PS, as suggested by the arance of the different parts shown in Fig. 6.11

Chap. 9, we will discuss the properties of rubbers. These are net-s, composed of chemically cross-linked macromolecules. Owing to the restoring forces, application of stress here induces a deformation that y large compared to solids. The observation of a plateau in the creep liance at a height comparable to the compliance of rubbers indicates a polymer melt actually resembles a temporary network. This behavior sses a major property specific for polymeric liquids: These include chain glements, i.e., constraints for the motion arising from the chain connec-, which act like cross-links. Different from true cross-links of chemical e, entanglements are only effective for a limited time during which they ble to suppress flow. This time becomes apparent in the creep curve as id of the plateau region.

bsequent to the plateau, flow sets in. As is intuitively clear, the time d for the chain disentangling increases with the molar mass and this up in a corresponding broadening of the plateau. Results of dynamic-anical experiments on polystyrene, presented later in Fig. 6.16, exemplify ehavior. The data also indicate a lower limit: When decreasing the molar one reaches a point, where the plateau vanishes. Then the glass–rubber tion and the terminal flow region merge together. Absence of the plateau s the absence of an entanglement network. The observation tells us that glement effects only exist above a certain minimum molar mass. For each ier one finds for that a characteristic value, known as the **molar mass e entanglement limit.**

ie measurements at high temperatures in Fig. 6.11 indicate a viscous vith a constant creep rate, determined by a viscosity η_0

$$\frac{\mathrm{d}J}{\mathrm{d}t} \propto \frac{1}{\eta_0} \,. \tag{6.95}$$

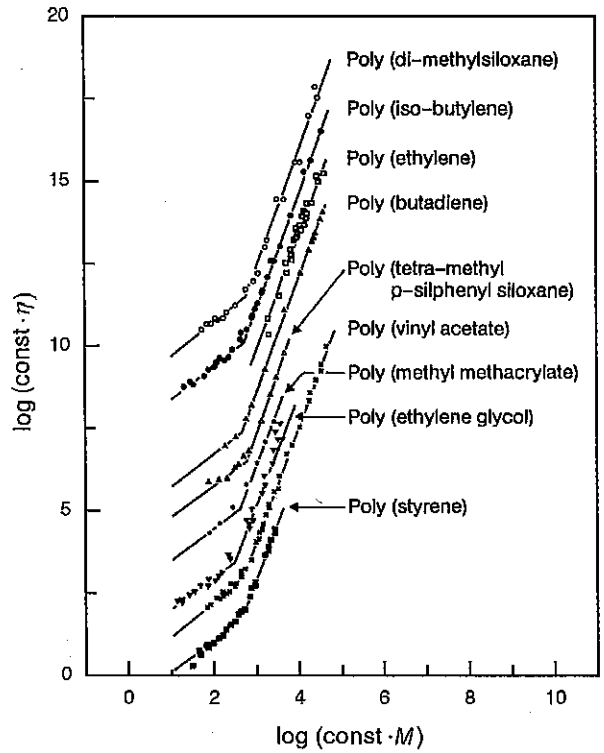

Fig. 6.13. Molecular weight dependence of the viscosity as observed for the indicated polymers. For better comparison curves are suitably shifted in horizontal and vertical directions. Data from Berry and Fox [71]

As the flow velocity relates to the disentangling time, this also holds for the melt viscosity. Indeed, η_0 and the disentangling time for entangled melts show the same dependence on the molar mass. Figure 6.13 collects the results of viscosity measurements for various polymers. As should be noted, a power law behavior

$$\eta_0 \propto M^{\nu} \tag{6.96}$$

is generally observed. One finds two regions, with different values of the exponent ν and a cross-over at a **critical molar mass** M_c. For molar masses below M_c one has $\nu = 1$; above M_c one observes $\nu \approx 3.2-3.6$. If viscosity measurements are further extended, up to the range of ultra-high molar masses, one finally observes an exponent $\nu = 3$. Figure 6.14 presents such measurements for 1,4-polyisoprene (PI), for molar masses up to $\overline{M}_w = 3 \times 10^6\,\mathrm{g\,mol^{-1}}$.

Importantly, as is also shown by Fig. 6.16, the two parts of the mechanical response separated by the rubber-elastic plateau differ in their molar mass dependence. In contrast to the terminal flow region, the glass–rubber transi-

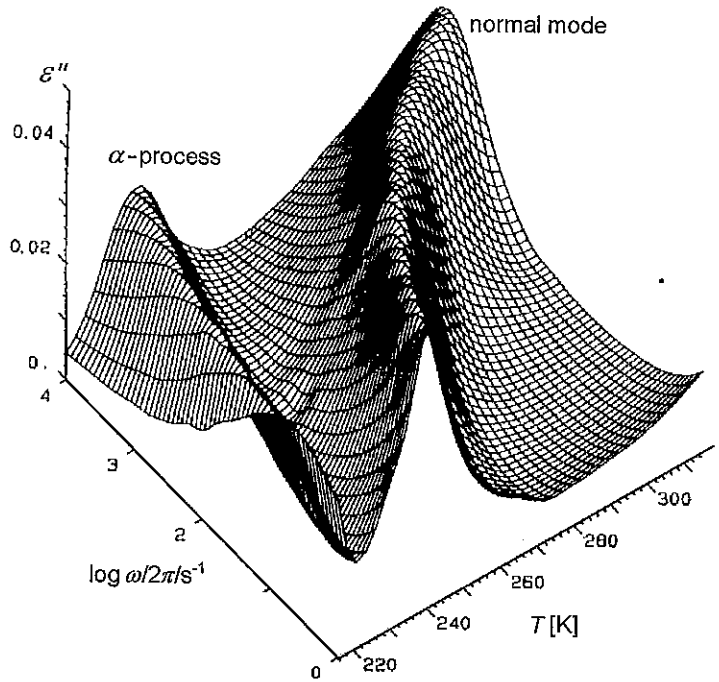

Fig. 6.20. Frequency dependence and temperature dependence of the dielectric loss in *cis*-PIP ($M = 1.2 \times 10^4\,\mathrm{g\,mol^{-1}}$), indicating the activity of two groups of relaxatory modes. Spectra obtained by Boese and Kremer [78]

focus in particular on the associated dipole moments. Figure 6.23 displays the chemical structure. The main point is that isoprene monomers are polar units that possess a longitudinal component $p_{||}$ of the dipole moment, which always points in the same direction along the chain. As a consequence, the longitudinal components of the dipoles of all monomers become added up along the contour, giving a sum proportional to the end-to-end distance vector $\boldsymbol{R}$. In the dielectric spectrum the kinetics of this total dipole of the chain is observable, hence also the chain reorientation as described by the time dependence $\boldsymbol{R}(t)$.

The peculiar name 'normal mode' needs a comment. As will be explained in detail in the next chapter, chain dynamics in melts may be described with the aid of two theoretical models known as the Rouse model and the reptation model. In the framework of these treatments chain kinetics is represented as a superposition of statistically independent **relaxatory normal modes**. As it turns out, the dielectric normal mode is associated with the mode with the longest relaxation time. For non-entangled melts this is the lowest order Rouse mode; for entangled melts, it is the lowest order reptation mode.

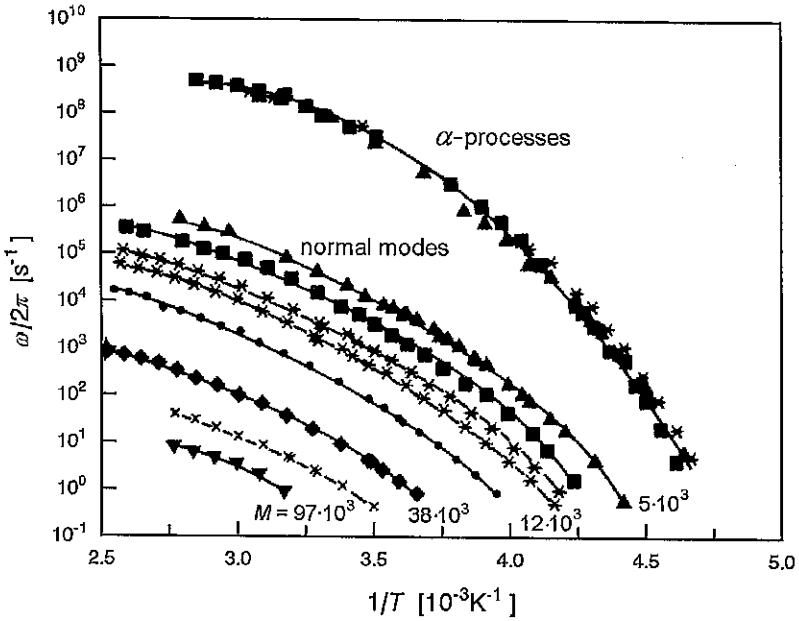

Fig. 6.21. Temperature dependence of the relaxation rates of the dielectric α-process and the normal mode, observed for samples of *cis*-PIP with different molar mass (four values are indicated). The *solid lines* are fits based on the WLF equation. Data from Boese and Kremer [78]

In addition to the longitudinal component of the dipole per monomer, there is also a transverse part. As the reorientation of the transverse component requires only local changes in the conformation, it can take place much more rapidly than the spatially extended normal mode. Hence, a qualitative change in the kinetics occurs and indeed, it is this movement that shows up in the α-process. Both the α-process and the normal mode obey the Vogel–Fulcher law, in full analogy to the common behavior of the α-process and the terminal relaxation in mechanics.

It is possible to write down approximate expressions for the relaxation strengths $\Delta\varepsilon$ of the two processes. As a chain may be described as a sequence of freely jointed segments, we can just make use of Eqs. (6.16) and (6.59), and introduce for the α-process and the normal mode the transverse and the longitudinal component of the dipole moment, respectively. The relaxation strength of the α-process then follows as

$$\varepsilon_0 \Delta\varepsilon_\alpha \simeq c_s \frac{\langle (p_\perp^s)^2 \rangle}{3kT} \,. \tag{6.131}$$

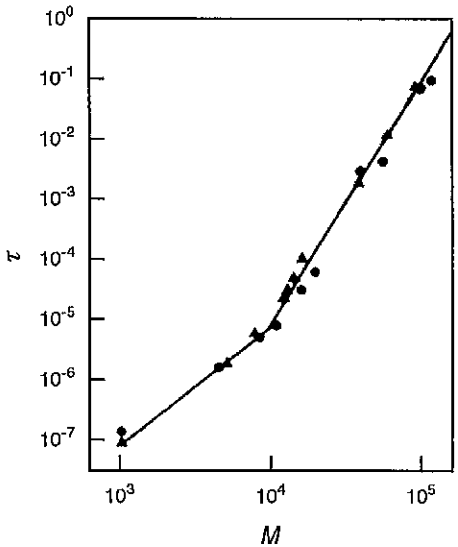

Fig. 6.22. Molecular weight dependence of the relaxation time of the dielectric normal mode in *cis*-PIP. Data from Boese and Kremer [78]

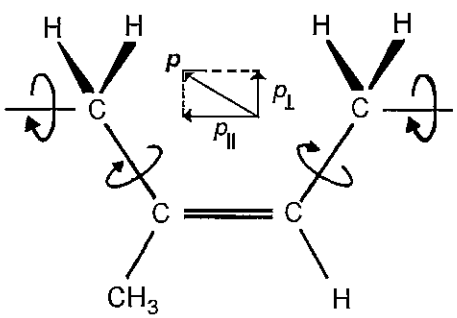

Fig. 6.23. Stereochemical constitution of a monomer unit of *cis*-PIP. The electric dipole moment, split into a longitudinal and a transverse component, is indicated

Here, $p_\perp^s$ is the transverse dipole moment per segment, and c_s gives the number density of segments. The brackets indicate an averaging over all rotational isomeric states of one segment. The relaxation strength of the normal mode follows equivalently, by introduction of the mean longitudinal dipole moment per segment

$$\varepsilon_0 \Delta\varepsilon_{nm} \simeq c_s \frac{\langle (p_\parallel^s)^2 \rangle}{3kT} \,. \tag{6.132}$$

Neither the α-process nor the normal mode equal a single-time relaxation process. A good representation of data is often achieved by the use of the empirical **Havriliak–Negami equation**, which has the form

$$\varepsilon - \varepsilon_u = \frac{\Delta\varepsilon}{(1 + (-i\omega\tau)^{\beta_1})^{\beta_2}} \,. \tag{6.133}$$

This function is a formal generalization of the single-time relaxation function, achieved by an inclusion of two additional parameters, β_1 and β_2 (for $\beta_2 = 1$ it equals the Cole–Cole function mentioned earlier). These determine the asymptotic behavior, β_1 on the low frequency side, since

$$\beta_1 \approx \frac{d \log \varepsilon''}{d \log \omega} \qquad \text{for } \omega\tau \ll 1 \,, \tag{6.134}$$

and the product $\beta_1\beta_2$ on the high frequency side, since

$$\beta_1\beta_2 = -\frac{d \log \varepsilon''}{d \log \omega} \qquad \text{for } \omega\tau \gg 1 \,. \tag{6.135}$$

Obviously β_2 determines the curve asymmetry. It is needed for the data representation because the observed curves $\varepsilon''(\omega)$ generally exhibit a larger broadening on the high frequency side. Typical values are $\beta_1 \simeq 0.5$, $\beta_2 \simeq 0.7$ for the α-process and $\beta_1 \simeq 1$, $\beta_2 = 0.4$ for the normal mode.

Equations (6.131) and (6.133) together provide a description of the dielectric α-transition, with the assumption that dipoles of different segments reorient independently. In fact, this is only true at larger distances from the glass transition temperature. On approaching T_g deviations show up. Figure 6.24 shows the temperature dependence of the relaxation strength of poly(vinylacetate) and one observes a pronounced increase. The behavior indicates increasing correlations between the motions of the transverse dipoles, not only along one chain, but possibly also between adjacent segments on different chains.

6.3.3 The Glass Transition Temperature

The mechanical experiments clearly demonstrate that the transition from the glassy to the liquid state is a purely kinetical phenomenon. Whether the compliance of a sample is small as in a glass, or large as for a rubber, depends only on the measuring time or the applied frequency. The reasons were discussed above. Rubber elasticity originates from the activity of the α-modes, a major group of relaxation processes in polymer fluids. The establishment of the deformation subsequent to the application of a load requires a certain time, given by the time scale of the α-modes. If the load varies too rapidly, the deformation cannot follow and the sample reacts like a glass. We also discussed the effect of temperature and found, as a main property of the α-modes, that relaxation times change according to the Vogel–Fulcher law. The progressive

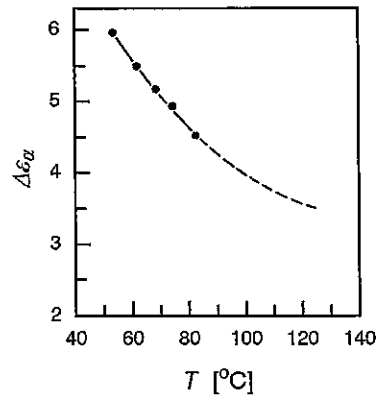

Fig. 6.24. Temperature dependence of the relaxation strength $\Delta\varepsilon_\alpha$ of the dielectric α-process in PVA. Data from Ishida et al. [76]

increase of the relaxation times on cooling implied by this law finally leads to a freezing of the α-modes within a comparatively small temperature range. If they are frozen, we have a glass.

We thus find glass-like reactions for both sufficiently high frequencies and sufficiently low temperatures; but are the two situations really comparable? The answer is, yes and no, depending on the point of view. Yes, because both situations have in common that the α-modes cannot equilibrate. No, if we consider the thermodynamic state of order. In the first case, we are dealing with a system in thermal equilibrium and study its reaction on perturbations; in the second situation, however, the system has become non-ergodic, i.e., thermal equilibrium is only partially established. A major part of the internal degrees of freedom, as represented by the α-modes, cannot equilibrate. The temperature, where the transition from a liquid equilibrium state to a non-ergodic one, i.e., only partially equilibrated state takes place, is called the **glass transition temperature**, with the general designation T_g.

How can T_g be determined? In principle this can be achieved in various ways. However, two of the methods are of special importance and are used in the majority of cases. These are temperature-dependent measurements of the expansion coefficient or the heat capacity of a sample, carried out during heating or cooling runs. They need only small amounts of material, and standard equipment is commercially available.

Figures 6.25 and 6.26 present as examples the results of a volumetric and a calorimetric measurement on poly(vinylacetate). The glass transition has a characteristic signature that shows up in the curves. As we can see, the transition is associated with steps in the expansion coefficient $\mathrm{d}\rho^{-1}/\mathrm{d}T$ and the heat capacity $\mathrm{d}\mathcal{H}/\mathrm{d}T$, i.e., changes in the slope of the functions $\rho^{-1}(T)$ and $\mathcal{H}(T)$. The transition extends over a finite temperature range with typical

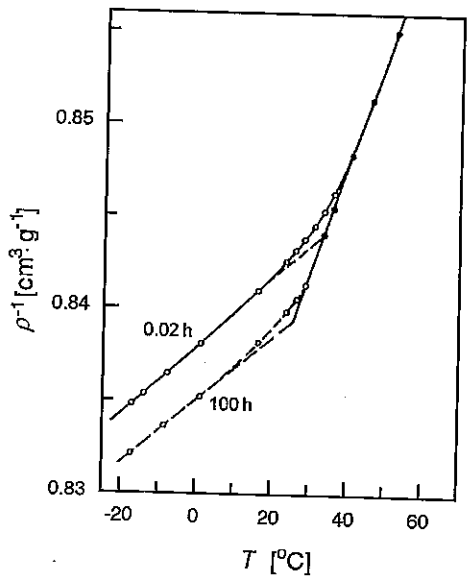

Fig. 6.25. Temperature dependence of the specific volume of PVA, measured during heating. Dilatometric results obtained after a quench to −20 °C, followed by 0.02 or 100 h of storage. Data from Kovacs [79]

widths in the order of 10 degrees. The calorimetric experiment also exhibits another characteristic feature. One can see that the location of the step depends on the heating rate $\dot{T}$, showing a shift to higher temperatures on increasing the rate.

In view of the broadening of the step and the rate effects, it does not seem appropriate to introduce a sharply defined T_g. For practical use as material parameter and for comparisons it is sufficient to conduct the measurements with a standard heating or cooling rate ($|\dot{T}| = (10^{-1} - 1)\mathrm{K\,s^{-1}}$) and to pick out some temperature near the center of the step, for example, that associated with the maximum slope. The thus obtained values of T_g have a tolerance of some degrees, but this must be accepted regarding the physical nature of the phenomenon.

The cause for the occurrence of the steps in the heat capacity and the expansion coefficient is easily seen. Cooling a sample below T_g results in a freezing of the α-modes. The observations tell us that the α-modes affect not only the shape of a sample, but also its volume and its enthalpy. This is not at all surprising. If segments move, they produce an additional volume in their neighborhoods. In the literature, this is often called a **free volume** in order to stress that it is not occupied by the hard cores of the monomers. The free volume increases with temperature because motions intensify, that

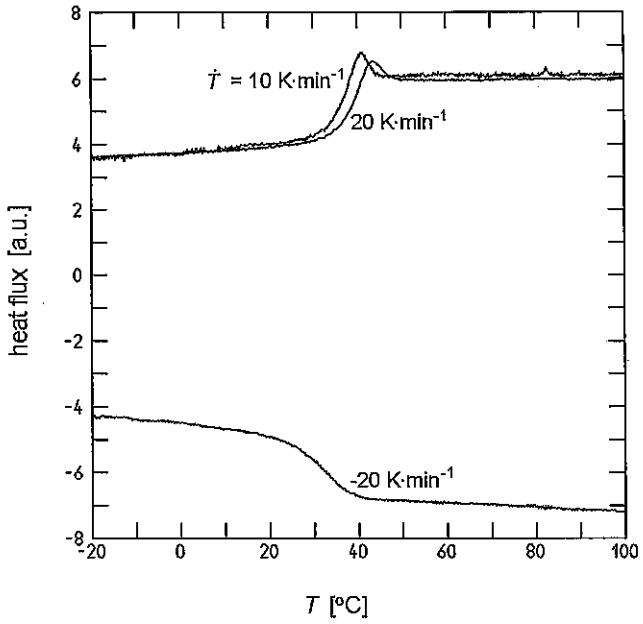

Fig. 6.26. Heat capacity of PVA, as measured in a differential calorimeter during heating (with two different heating rates) and cooling

is to say, the jump rates increase and, more importantly, a growing number of conformational states becomes populated and not all of them allow a dense chain packing. Therefore, when on crossing T_g from low temperatures the α-modes become active, beginning slowly and then steadily increasing in intensity, a growing additional free volume correspondingly arises. Thermal expansion in the glass is due to the anharmonicity of vibrational motions, as in crystalline solids. As we can see, the α-modes contribute another, even larger part to the expansion coefficient and it comes into effect at T_g.

That a corresponding behavior is found for the enthalpy and the heat capacity is conceivable. As the free volume incorporates energy, changes in the volume and in the enthalpy are interrelated and this results in simultaneous steps in the expansion coefficient and the heat capacity.

Being in a non-equilibrium state, liquids below T_g have a tendency further to change the structure in the direction towards the equilibrium. A slow decrease in volume and enthalpy is often observed. Figure 6.25 also exemplifies this behavior. Prolonged storage of the sample of poly(vinylacetate) below T_g for 100 h results in a shrinkage in volume. Note that, as a consequence, T_g, as measured during the subsequent heating, is shifted to lower values. Formally, this may be associated with the shift of the point of intersection of the two lines representing the glassy and liquid state. Physically, it is caused by

a change in the microstructure. Ag
for these processes and they can pr
properties deteriorate.

We have seen that the position
the heat capacity, observed during
It is possible to analyze this depen
rion for the location of the glass tra
when cooling a polymeric liquid. In
libriate rapidly so that thermal eq
change on approaching the glass t
of the α-modes reach values that
tinuous equilibriation. Vibrations
programmed temperature changes
and more. Finally, after having cr
change between the instantaneous
completely.

In an analysis, one has to co
processes under non-isothermal c
heating run. Observations suggest
a sum of two contributions

$$\mathcal{V}(T) = \mathcal{V}$$

The first part $\mathcal{V}_u$ describes the vo
modes, being determined by the ha
ity of the vibrations and possible
second term $\Delta\mathcal{V}_\alpha$ accounts for th
An analogous description is sugge
correspondingly as

$$\mathcal{H}(T) = \mathcal{H}$$

Since $\mathcal{V}_u(T)$ and $\mathcal{H}_u(T)$ pass contin
any peculiar effects, we may reduc
α-modes. To keep the equations sim
of the α-process and assume a sing
dependence following the Vogel–F
by an application of the relaxation

$$\frac{d\Delta\mathcal{H}_\alpha}{dt} = -\tau_\alpha^{-1}($$

which is formulated here for the c
equation, the change from a non-
ated with the α-modes, $\Delta\mathcal{H}_\alpha$, to t
a temperature-dependent rate τ_α^{-1}